Molecular-hydrogen laser: 1098–1613 Å†

R. W. Dreyfus and R. T. Hodgson
IBM Thomas J. Watson Research Center, Yorktown Heights, New York 10598
(Received 26 November 1973)

A 4-GW electron beam has been used to excite amplified spontaneous emission in hydrogen isotopes (ortho and para H_2, HD, and D_2). The laser energy has been measured with photodiodes, an ionization chamber, and film, and these different measurements are compared in detail. Analysis of the laser energy indicates the spectral linewidth is due to Doppler broadening, and, consequently, cooling the gas produces higher gain and power. This additional gain allows lasing to be observed at even shorter wavelengths (1098 Å as compared to 1161 Å) than reported previously. Also many (stimulated emission) spectral lines of the Werner and Lyman bands are reliably identified for the first time.

I. INTRODUCTION

Laser action in the ultraviolet[1-3] (uv) and the vacuum ultraviolet[4-6] (vuv) spectral regions can be produced by relativistic electron beams traveling through gases. The high-energy primary, secondary, and cascade[7] electrons collide inelastically with gas molecules and excite bound electrons to high-energy states (see Fig. 1). A population inversion results because the upper vibrational levels ($v'' > 0$) of the ground electronic state are initially empty and have very low probability of being excited. References 5 and 8 describe the present experimental arrangement for exciting gases (primarily H_2 at 25-Torr pressure) by propagating gigawatt electron beams several meters through the gases. This arrangement may be considered as the electron beam (e beam) equivalent to longitudinal optical pumping, as contrasted to transverse[9] electron-beam excitation, which is the analog of the usual optical-pumping scheme.

This paper gives details of the hydrogen laser which were not contained in the previous brief communications. These details involve comparisons of the calculated and measured output energies, the temperature dependence of the output energy, the identification of weaker laser lines, and the effects of isotopic substitutions for H_2. Section II describes the experimental arrangement. Section III gives the spectral line identification and the results of laser energy measurements. A quantitative discussion of the present laser is given in Sec. IV. The Appendix derives the expressions which describe the transfer of energy from the electron beam to laser light.

The present laser operates in the amplified spontaneous-emission (ASE) mode, just as does the molecular-nitrogen laser, since there are no mirrors to provide feedback. Figure 2 shows the laser tube subdivided according to the locally dominant amplification process. Region I acts as the noise source, i.e., it is the region in which the light is essentially that produced by spontaneous emission of radiation. Region II exhibits unsaturated gain, i.e., the photon flux is too low to affect significantly the inversion density. In region III the photon flux has become sufficient to deplete the population inversion.

By modeling and analyzing this vuv laser, we hope to attain several goals. A primary objective is to increase the power in the Werner-Band radiation above the previously reported[5] 500 W/cm^2 at 1161 Å. Increases in power are available by increasing the cross section for stimulated emission of photons. The cross section is (presumably) increased by cooling the laser gas to decrease the Doppler linewidth.

A second goal involves substituting other gases for H_2 in the present laser. One then has a choice of a number of wavelengths from a single piece of equipment.[6] Furthermore, substitution of the heavier isotope, deuterium, provides a decisive check on the Doppler-broadening hypothesis. The pulsed nature of the present e-beam excitation makes it necessary to verify that line broadening does not arise from other sources, such as from the very large magnetic and electric fields present in the laser tube.

II. EXPERIMENTAL ARRANGEMENT

The over-all layout of the present equipment has been discussed in Ref. 5. Here we shall be more specific and shall concentrate on the details of e-beam propagation and on recent modifications to cool the laser gas and to measure the output energy W_l.

A. Relativistic e-beam propagation

The source of the ~1-cm^2, 10-kA electron beam is a field-emission diode powered by a 600-kV

pulser.[10] We are interested in the propagation of these beams for large distances (meters) through gases maintained at the highest pressure in which the beam will propagate.

Normally, high-current e beams diverge due to self electrostatic repulsion. However this effect is negligible once ionization of the laser gas has supplied space charge to neutralize the space charge of the beam electrons (only $\sim 2\times 10^{12}$ ions/cm^3 are required).

One source of beam divergence is repeated, low-angle electron-molecular scattering.[11] At not too-high gas pressures, uniform beam propagation can be maintained since these collisions are counterbalanced by the two stabilizing magnetic fields discussed below. Actually, the present beam current is intermediate between the low current which produced divergence owing to scattering and the high current which produced (radial) electrical breakdown in the gas.[11] Thus, it is not yet possible to ascertain which effect limits the usable gas pressure. For hydrogen the maximum laser energy is obtained with a gas pressure of 25–30 Torr at 296 °K and with 8 Torr with liquid-nitrogen cooling; obviously these conditions represent similar gas densities.

The magnetic field due to the e-beam current itself is in the ϕ direction, as shown in Fig. 3. The effect of this field is to promote the self-focusing electron trajectories shown.

The electron beam also propagates down the flux lines of an externally applied z-axis field.[5] This field is known empirically to aid beam propagation. Qualitatively, one can say that this field bends the r, ϕ components of electron velocity into spirals, so the diverging electrons (both primary and secondary) are restrained from reaching the laser-tube walls.

B. Laser tube

The stainless-steel laser tube fulfills a number of functions in addition to simply containing the laser gas. These functions are to provide a return-current path for the e-beam pulse, to physically support the external magnetic-field solenoid, and to guide the e beam down the same axis as the light. The walls of the laser tube are cooled to cool the laser gas to ~90° so as to narrow the (Doppler-broadened) spectroscopic lines. The above functions are fulfilled by the design shown in Fig. 4. The effects of tube radius have not been fully explored. Early experiments[2,4,5] indicated that a 2-cm inner diameter produced less laser energy, however, the study has not been extended beyond this one comparison.

The external magnetic field is powered by a 400-μF, 4-kV (maximum) capacitor bank. Optimum magnetic fields are 6 and 13 kG, at 90 and 296 °K, respectively. In the laser-tube construction, care is taken to minimize inductively induced currents, which produce inhomogeneities in the magnetic field.

The gases used are Research-Grade. Impurities, including outgasing, are estimated to have a maximum partial pressure of 10 mTorr in the laser tube. Assuming typical continuum optical-absorption cross sections of 3×10^{-17} cm^2 for these impurities gives an absorption coefficient of 0.01 cm^{-1}. Although this absorption is significantly smaller than the largest gains calculated in Sec. IV, impurities may possibly have some effect upon the lines with low gain.

The uv light from the laser tube is filtered or attenuated by two techniques. Short-wavelength cutoff occurs by means of the exit window, which is either LiF or Al_2O_3. These limit the short wavelengths to about 1050 and 1420 Å, respectively. It is possible to operate the laser in a windowless

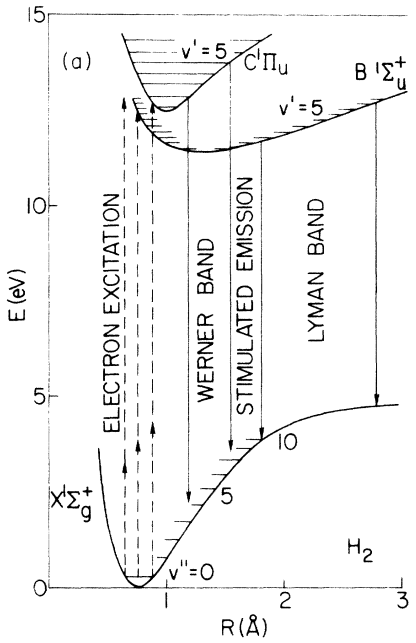

FIG. 1. Potential-energy curve for the $X^1\Sigma_g^+$, $B^1\Sigma_u^+$, and $C^1\Pi_u$ states of H_2. Only the $(v''=0)$ $X^1\Sigma_g^+$ state is occupied before electron-beam excitation. Note that lasing must occur in a time comparable to the $B\rightarrow X$ or $C\rightarrow X$ spontaneous-fluorescence time, otherwise the upper vibrational states of the $X^1\Sigma_g^+$ manifold will be occupied and the gas will act as an absorber. The rotational substates possess too small energy spacings to appear on the present figure. The $Q1$ rotational line of the $(v'=1)\rightarrow(v''=4)$ transition is the strongest line in the present Werner-band emission; this transition will be identified as the (1-4) $Q1$ Werner line.

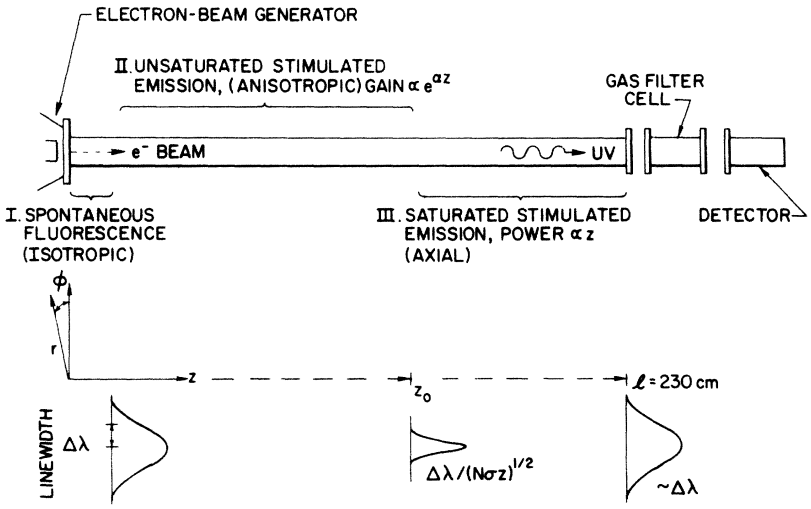

FIG. 2. Different parts of the laser tube as delineated by the predominant amplification process in each part. Since the amplification depends upon which spectral line one is discussing, the different areas will occupy different fractions of the laser tube for different spectral lines. The radiation linewidth is indicated near the bottom of the figure and makes several transitions. In region I, the linewidth has the ordinary Doppler breadth; near z_0 the linewidth is gain-narrowed to $\Delta\lambda/(N\sigma z_0)^{1/2}$, and at $z \gg z_0$, hole burning combined with saturated-gain behavior increases the linewidth back to $\sim\Delta\lambda$. The quantity N is the net inversion density as defined by Eq. (A3) and σ is the cross section for stimulated emission.

mode by filling the spectrograph[4,5] with the same gas as the laser tube. This was done in the (unsuccessful) searches for lasing transitions at $\lambda < 1050$ Å.

Gas cells, either 12 or 1.32 cm long, may be inserted between the laser and the optical detectors discussed below. The gas filter attenuates the laser output by known amounts, so that the detectors operate in their linear ranges. Typical filling gases are triethylamine (TEA), methane, and oxygen.[12]

C. Optical detectors and power measurements

Three optical detectors have been used, namely, photographic film, photodiodes, and an ionization chamber. These detectors measure slightly different quantities: film measures energy per cm^2 at each wavelength, the photodiodes measure power (which integrates to give energy), and the ionization chamber measures energy. With all these techniques, the energy per cm^2, W_l, is best expressed as photons per cm^2, since this basically is the quantity measured and the dependence of photon energy upon λ is removed. It does not appear practical to say that any one power-measurement technique is better than another. For future applications, each technique is noted to have advantages and disadvantages.

Either short wavelength radiation (SWR) or SC7 film[13] was used in a McPhearson model 225

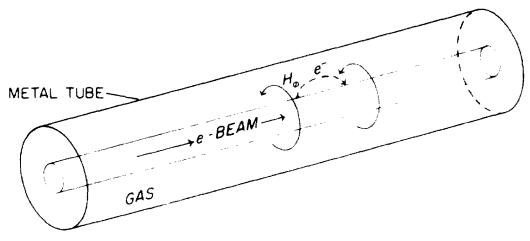

FIG. 3. H_ϕ magnetic field generated by the e-beam itself. Note that this field bends the individual electrons into a pinched beam. The interaction of H_ϕ with the conducting tube walls is repulsive; hence this force tends to center the entire beam on the $r=0$ axis.

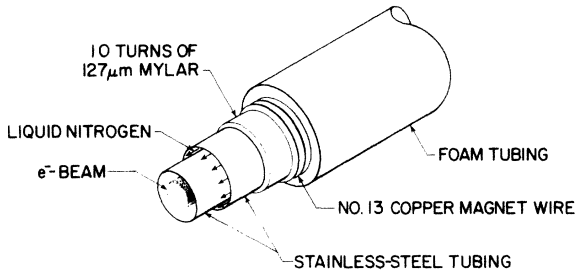

FIG. 4. Cross-sectional view of the laser tube; note the annular space through which liquid nitrogen flows. The diameters of the tube are inner stainless-steel tube, 0.384-in. inner diameter, 0.500-in. outer diameter; outer stainless-steel tube 0.634-in. inner diameter, 0.750-in. outer diameter; and Armoflex (Ref. TM) foam tubing, 0.875-in. inner diameter and 1.875-in. outer diameter. The thermal jacketing is sufficient for liquid nitrogen to flow the 2.3-m length with a consumption of only ~3 liter/h.

spectrograph. The former is finer grained, ~1 μ, however, there is some question[14] as to its aging and reproducibility. The calibration of SC7 is available,[15] but one must contend with a grain size and fog level several times larger than with SWR film. A few test exposures with nanosecond pulses from a conventional nitrogen-gas laser gave no indication of reciprocity failure with SC7 film. Also, as will be seen later in Fig. 6, the γ of the film is the same for nanosecond exposures as for conventional exposures. This film is consequently utilized for quantitative measurements.

While the sensitivity of the film is reasonably (within[15] a factor of 2) well established, it is useful to check the energy output by other techniques also. One of the reasons for this cross checking is that the film is utilized in a 1-m spectrograph where the grating efficiency is *estimated*[16] to be 60% at 1600 Å and 40% at 1200 Å.

Two photodiodes have been utilized with the present spectrometer. A planar diode, identified as No. 1, with LiF window and molybdenum photocathode detects the power for $\lambda > 1050$ Å. The response is less than 0.3 nsec when driving a No. 519 Tektronix oscilloscope. While this photodiode has short-wavelength and response-speed capability, it also has some rather significant disadvantages. There are uncertainties in the sensitivity of the photocathode since we are operating near the long-wavelength threshold[16] for molybdenum. Even though this photocathode is supposedly insensitive at $\lambda > 1400$ Å, attenuation of the light beam with methane, which cuts off wavelengths less than 1400 Å, still gives a significant signal. This implies some sensitivity remains, possibly either due to an intense line at 1402.65 Å or the very intense Lyman-band lines near 1600 Å. This spurious signal indicates that a spectrometer must be utilized even with this photodiode if only a narrow spectral region is to be measured. This inclusion of a spectrometer means that when photodiode No. 1 is utilized for Werner-Band measurements, the grating efficiency had to be estimated at 40% near 1200 Å. Also, the LiF photodiode-window transmission is only 55% at 1161 Å. Care must be exercised to avoid fast electrons hitting the LiF window, otherwise the transmission is decreased rapidly.[17]

The 1600-Å photodiode, No. 2, also has a planar configuration, but with a sapphire window and an S20 photocathode.[18] The response time is 1.2 nsec in the present holder with the No. 519 oscilloscope. The sapphire-window transmission is estimated[19] to be 40% near 1600 Å. This factor is combined with the manufacturer's uv calibration to give a calibration for the vuv region. The sapphire-window limits[19] the sensitivity to $\lambda > 1420$ Å.

An ionization chamber sums the laser energy over a given spectral region, see Fig. 7.48 of Ref. 16. The ionization chamber has a conventional coaxial geometry, 13 cm long with a LiF end window. In order to collect all the ions, one must operate at filling pressures less than 1 Torr. At

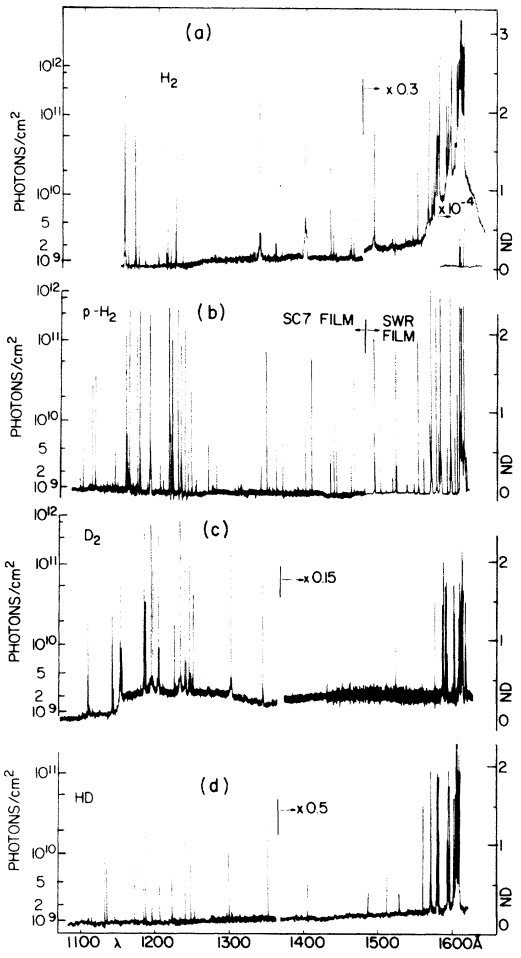

FIG. 5. Composite of densitometer traces of H_2, para-H_2, D_2, and HD spectra. Each spectrum is recorded in two shots, one for each ~400-Å spectral region covering the Lyman bands (1300–1700 Å) and the Werner bands (1100–1500 Å). The line intensities in the overlap region are measured for each isotope and used to estimate the difference in power between the two shots. These differences are recorded at the break between each two spectra. (a) H_2 spectrum: $T \approx 90$ °K, 8-Torr H_2 pressure. The insert is a densitometer tracing of a shot attenuated $\approx 10^4$ times with molecular oxygen. (b) p-H_2 Werner-band spectrum taken with the para H_2 cooled with liquid helium. Pressure is ~2 Torr. Lyman band recorded using Kodak SWR film with room-temperature gas and 25-Torr pressure. (c) and (d) D_2 and HD spectra recorded with gas at ≈ 90 °K and at 8-Torr pressure.

TABLE I. Wave number and identification of observed stimulated-emission lines[a] for hydrogen isotopes [logarithms of (photon density)/cm^2 given in parentheses].

(A)

H_2 Werner bands ($C\,^1\Pi_u - X\,^1\Sigma_g^+$)

	p-H_2			H_2	
v'-v''	$R0$	$P2$	$Q1$	$P3$	$R1$
0-2	91 061(9)	90 740(9.5)			
0-3	87 365(9.8)	87 061(9.2)			
1-3	89 674(10.3)	89 370(10.4)			
1-4	86 205(11.1)	85 918(11.7)	86 109(11.3)	85 747(10)	
1-5	82 963(9.3)	82 693(9.2)	82 873(9.3)		
2-5	85 138(11.1)	84 868(11.4)	85 048(10.7)	84 707(10.7)	
2-6	82 124(11.6)	81 871(11)	82 039(10.6)	81 727(9.7)	82 150(9.3)
3-6			84 082(9.1)		
3-7	81 384(11.6)	81 149(11)	81 305(10.8)		
3-8	78 840(9.7)				
4-8	80 754(11.2)	80 537(9.7)	80 681(10.5)		
5-9	80 244(10.4)				
6-10	79 871(9.3)				

H_2 Lyman bands ($B\,^1\Sigma_u^+ - X\,^1\Sigma_g^+$)[b,c]

	p-H_2				H_2	
v'-v''	$P4$	$P2$	$R0$	$P3$	$P2$	$P1$
0-3		78 158(9.6)				
0-4		74 707(10.7)		74 501(11.2)		
0-5	71 059(10.4)	71 482(10.3)		71 294(10.9)		
0-6	68 101[b]	68 485(9.4)		68 314(10.5)		
1-6		69 802(9.3)		69 627(10.3)		
1-7		67 037	67 271	66 880(10.7)		
1-8		64 512	64 728	64 373(10)		
2-8		65 792				
2-9		63 519		63 396(10.8)		
3-7		69 562(10)		69 399(9.4)		
3-10	62 529	62 759	62 933	62 654(12.9)	62 758(10.3)	62 841(11.3)
4-6		73 538(9.5)				
4-9		65 976		65 847(9)		
4-11	60 752	60 869	60 993	60 813(13.8)	60 869(12.3)	60 919(12.7)
5-10		65 149				
5-12	61 925	62 048	62 172	61 989(14)	62 048(12.9)	62 099(13)
6-7		73 100(9.6)				
6-9		68 301(10.3)		68 168(9.8)		
6-13	62 127	62 178	62 269[b]	62 149(13.5)	62 178[b]	62 208(13.1)
7-9		69 415(9.7)				
7-13		63 292	63 384	63 261(12.9)	63 292(11)	63 324(11)
8-14	63 839[b]	63 795	63 845[b]	63 806(10.8)		

(B)

HD Werner bands ($C\,^1\Pi_u - X\,^1\Sigma_g^+$)

v'-v''	$R0$	$P2$
1-4	87 824(10)	87 601(9.7)
1-5	84 885(9.9)	
2-5	86 807(8.8)	
2-6	84 037(10.3)	83 836(10.1)
3-7	83 262(9.3)	
4-8	82 559(9.7)	
6-10	81 409(9.7)	

TABLE I *(Continued)*

(C)

HD Lyman bands ($B\,^1\Sigma_u^+ - X\,^1\Sigma_g^+$)

$v'-v''$	$R0$	$P3$	$P2$	$P1$
0-3			79 824(9.9)	
0-4			76 726(10)	
0-5			73 797(10.3)	
0-6			71 038(9.6)	
1-8			67 185(9.4)	
2-9			66 068(9.6)	
2-10			64 020(10.5)	
3-11		63 169(10.7)	63 257(10)	
4-12		62 601(10.5)	62 677(10.7)	62 744(9.8)
5-11			65 364(9.3)	
5-13	62 409(10.3)	62 237[b]	62 298(11.3)	62 357(10.4)
6-5			80 278(10.2)	
6-14	62 238[b]	62 100(10.7)	62 146(10.9)	62 192(10.7)
7-15	62 319[b]	62 223[b]	62 248[b]	
8-15	63 288(9.7)	63 190(10.7)	63 217(10.7)	
9-16	63 639(9.5)	63 586[b]	63 591[b]	

D_2 Werner bands ($C\,^1\Pi_u - X\,^1\Sigma_g^+$)[a,d]

$v'-v''$	$P2$	$R0$
1-4		89 818(10.3)
1-5	87 141(9.5)	87 897(10.9)
2-6	86 326(9.8)	86 468(11.1)
2-7	84 030(10.3)	84 167(11.2)
3-8	83 375(10.7)	83 505(11.3)
3-9		81 433(10)
4-9	82 767(9.7)	82 891(11.2)
4-10		80 935(11.3)
5-11	80 378(9.5)	80 490(10.7)
6-12	80 002(9.3)	80 108(10.7)
7-13		79 790(10.3)

D_2 Lyman bands ($B\,^1\Sigma_u^+ - X\,^1\Sigma_g^+$)[a,d]

$v'-v''$	$P3$	$P2$	$P1$	$R0$
0-5		76 709(9.3)		
0-6		74 300(9.7)		
0-7		72 005(9.8)		
0-8		69 824(9)		
3-13		63 458(10.2)		
4-14		62 900(10.3)		
5-15	62 418(10)	62 466(10.3)		
6-16	62 129(10)	62 168(10.4)	62 201(10.1)	
7-16		63 004(10.6)	63 038[b]	
7-17	61 987[b]	62 019[b]	62 046[b]	62 083[b]
8-17	62 804(9.5)	62 839(10.3)		
8-18	62 013[b]	62 034[b]	62 055[b]	
9-19		62 235[b]	62 247[b]	62 275[b]
9-20		61 859(10.1)		
10-19		63 023[b]	63 035[b]	

[a] Gas temperature and pressure are the same as in Fig. 5, namely, $T = 90\,^\circ$K, except for p-H_2 for which $T \ll 90\,^\circ$K.

[b] Energy values greater than 10^{12} photons/cm^2 are determined from the attenuated spectrum, cf. Figs. 5(a) and 6.

[c] H_2 Lyman-band wave numbers are by G. Herzberg and L.L. Howe, Can. J. Phys. 37, 636 (1959).

[d] D_2 wave number values of H. Bredohl and G. Herzberg, Can. J. Phys. 51, 867 (1973).

higher filling pressures, ion-electron attraction forms uncharged complexes. This problem is serious only at high ion-electron concentrations, e.g., in the case of pulsed-laser power measurement. Complexes represent the first step in recombination, but form much more rapidly than the complete recombination products. The less than 1-Torr gas pressure means that only (30–50)% of the laser light is absorbed.

The filling gas is nitric oxide (NO) for detection of $\lambda < 1342$ Å and TEA for $\lambda < 1653$ Å. The ionization probability is accurately known[20] for NO; unfortunately this is not the case with TEA and it had to be estimated at 10% from work on similar compounds.[21] This percentage may be in error by as much as a factor of 3.

III. EXPERIMENTAL RESULTS

The general objective of the present work is to understand the output energy and emission wavelengths of this longitudinally pumped, e-beam laser. The requisite information is primarily obtained from spectrographic film. This technique not only provides the wavelength, but also provides quantitative information about the laser energy when suitable attenuation is inserted in the optical path.

Microdensitometer tracings of the highest-intensity stimulated-emission spectra of the H_2 isotopes are reproduced in Fig. 5. Each spectrum is taken in two shots and recorded in two parts, usually 1100–1500 and 1300–1700 Å. The line intensities in the overlap region are measured for each isotope and used to estimate difference in total power on the two shots. These differences are recorded in Fig. 5 at the break between each two shots.

For comparison, the spectrum of para hydrogen, p-H_2 (1300–1650 Å), recorded on Kodak SWR film is shown. The ordinates in this case refer only to the Kodak Pathé SC7-film spectrum shown from ~1100–1300 Å. Note that the background (baseline) density is nearly flat for the SWR film when compared to the SC7 film. Also, the very intense lines still remain isolated from each other, because the smaller SWR-film grain size avoids some of the filling in between intense lines. The (0-2) $R0$ line is observed at 1098 Å; this represents the shortest-wavelength stimulated-emission line to date.

The wavelengths of the H_2-isotope stimulated-emission spectra are determined to an accuracy of 0.1 Å by comparison with H_2 Lyman-band and Werner-band spontaneous-emission spectra. The present Lyman-band emissions extend from about 1620 to 1275 Å, and the presently observed Werner-band transitions occupy the range from 1275 to 1098 Å. Specific line assignments given in Table I are derived from the theoretical energy-level calculations of Kolos and Wolniewicz.[22,23]

The H_2 spectrum contains an insert of a shot attenuated $\approx 10^{-4}$ times with an O_2 filter. The (5-12) P_3-line data (at 1613 Å) from such attenuated spectra are plotted in Fig. 6. A line corresponding to $W_l = 1.3 \times 10^{14}$ photons/cm^2 fits the data reasonably well; this illustrates the technique used to determine the energy in the more intense (>10^{12} photons/cm^2) spectral lines.

Three sources of uncertainty predominate when the laser energy is determined with this film-attenuator combination. First, there is a ±50% shot-to-shot variation in laser energy, a variation which will be more apparent later. The uncertainty in the SC7-film calibration has already been noted. A third uncertainty is the precise determination of the attenuation factor: the cross section for O_2 absorption is known[12] to about ±5%, which gives an uncertainty in W_l of $10^{4\pm0.2}/10^4 \approx 50\%$. Combining the three uncertainties means that this technique of laser-energy measurement is accurate only to within a factor of ≈3. (The film calibration and attenuation factor represent systematic errors and hence cannot be reduced by a large number of readings.) The strong 1613-Å Lyman line represents the worst case, as the Werner-band lines or weaker Lyman-band lines are subject to significantly less attenuation and

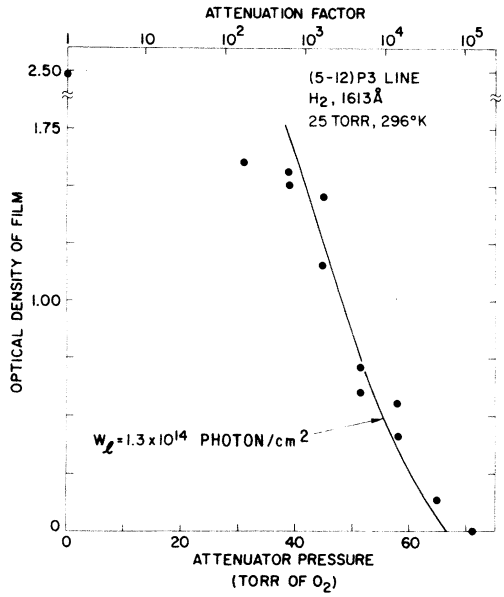

FIG. 6. Points give measured optical density vs oxygen attenuation for the (5-12) $P3$ Lyman line. The film exposure is calculated from Ref. 20 (with the attenuation factor calculated from the data compiled in Ref. 17).

associated uncertainty.

In Table I, the intensities of the lines and their order of appearance as the H_2-gas temperature is decreased are not surprising. To use H_2 as an example, the lines originating from ($v'=4, 5, 6$) $B^1\Sigma_u^+$ states and the ($v'=1, 2$) $C^1\Pi_u$ states are the strongest in the Lyman and Werner bands, respectively. (The downward transitions from these states appear primarily in the regions near 1600 and 1200 Å.) The above states have the largest Franck-Condon (FC) factors for excitation from the ($v''=0$) $X^1\Sigma_g^+$ ground state.[24] All excited states have highest gain on transitions with the largest FC factors, and these lines are correspondingly intense. In some cases, more than one line arises from a particular excited state. It appears probable that the downward transition with largest FC factor is saturated, and that the gain on another, unsaturated transition can be large enough to give significant amplification.

Figure 7 shows the ionization chamber (IC) signal versus the gas pressure in the attenuator. (The extrapolation to zero pressure gives the unattenuated signal, of course.) Several features are evident from the data in Fig. 7. First, the scatter of points around the straight lines indicate a ±50% shot-to-shot energy variation. Second, the increase in energy with cooling D_2 to 90 °K is also evident. The ionization chamber gave the best comparison of output energy, since these measurements were taken contiguously. The above increase at low temperature is particularly impressive in the case of D_2, since increased gain results from both the narrower lines and from only the lowest two rotational states being populated. (In H_2, even at 296 °K, ≈80% of the molecules are in the lowest two states, hence this second benefit is minor.) Third, TEA is a satisfactory attenuator; the attenuation per Torr calculated from Fig. 7 agrees within 5% with previous published results.[12] The last experimental feature is that the ionization chamber does not saturate at present energy levels when low filling pressures are utilized.

The values displayed in Fig. 7 are primarily due to Lyman-band radiation around 1600 Å; these values must be multiplied by a number of factors in order to estimate the actual laser energy. Among these factors are that only 50% of the photons are absorbed in the TEA in the IC; the ionization probability is estimated at 10%; the active laser area[25] is taken to be 0.2 cm^2; and there are reflection losses in the LiF windows. The average of several plots like Fig. 7 plus the above corrections give the energies listed in Table II(A).

When the ionization chamber is filled with nitric oxide, presumably one obtains laser energies corresponding only to photons with $\lambda \leq 1342$ Å [see Table II(B)]. Very little attenuation is required because of the much lower intensity of the Werner-band lines as compared to the Lyman-band lines. Radiation around 1600 Å still contributes a small background signal, perhaps due to an impurity present in the NO. One separates the desired and spurious signal by using methane as an attenuator, this gas is transparent near 1600 Å, but opaque for $\lambda \leq 1342$ Å.

Integration of the photodiode signals forms the third basis for determining W_l as given in Table II(A) and (B). Representative oscilloscope traces appeared in Ref. 6.

Table II summarizes the laser energy measurements for extended spectral regions and the two gas temperatures. Besides the shot-to-shot variation, the different detectors give values which range over nearly an order of magnitude. This is not surprising since the sensitivity of each detector is known only within a factor of ~3. While continuing effort should be made to minimize the uncertainties, this range is not prohibitive with respect to present purposes. The W_l values are used to evaluate the net inversion density and

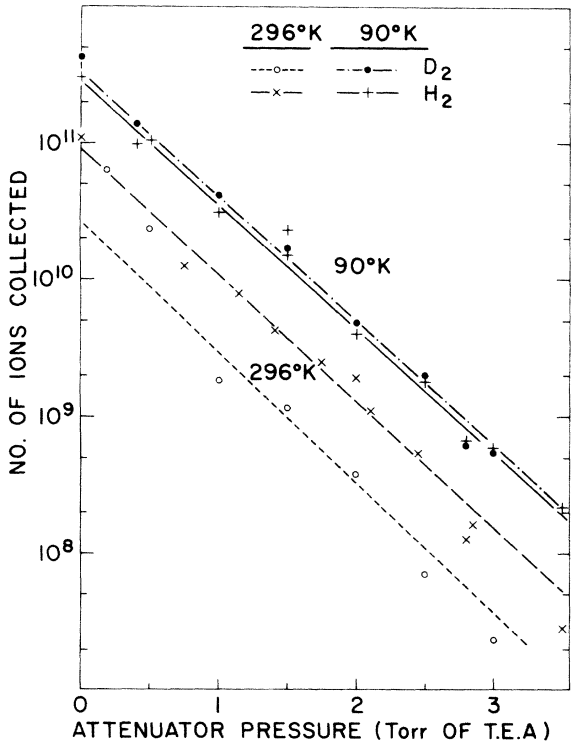

FIG. 7. Number of ions collected in the ionization chamber vs the gas-attenuator pressure. The attenuator is triethylamine (TEA). The ionization chamber is filled with TEA also, so that it is sensitive to $\lambda < 1653$ Å. A large increase in number of ions, and evidently laser energy, are observed when D_2 is cooled to ≈ 90 °K.

cross section for stimulated emission in Eq. (1) where these quantities appear as exponentials. An order-of-magnitude variation in W_l then causes only about a ±10% uncertainty in the measured gain coefficient α. The conclusion is that the present energy measurements are sufficient for testing the model proposed in the Appendix.

IV. DISCUSSION

Since the number of observed laser transitions is so large, we shall consider the gain and output energy in two exemplary cases only, i.e., unsaturated gain and then saturated gain. The Appendix provides the mathematical expressions for analyzing the present laser under both cases.

First the (1-4) $Q1$ Werner line (at 1161 Å) typifies laser operation in the unsaturated gain region, II. Equation (A5) of the Appendix, expresses the laser power p in terms of measurable quantities. The laser energy is derived by integrating p over the time span of the population inversion:

$$W(z) = \int_0^{t'(N=0)} p(z, t')\, dt' = \frac{r_0^2 A_{12}}{4\sigma^{3/2} l^2 z^{1/2}} \int_0^{t'(N=0)} \frac{e^{N\sigma z} - 1}{N^{1/2}}\, dt' \,. \qquad (1)$$

The output energy W_l for unsaturated gain is obtained by considering the entire laser tube, i.e., $z = l$, substituting the cross section for stimulated emission (σ) from Eq. (A10) and using Eq. (A14), to give the net inversion density $N(t')$. The most important factor in (1) is $e^{N\sigma z}$, which shows the amplification, $N\sigma$ per centimeter as the photons travel down the laser tube. The variable which is used to compare experiment and theory is the rate of excitation as given in (A14) by an effective cross section for excitation, σ_{e^-}. Note that $N \propto \sigma_{e^-}$. The remaining symbols in (1) are t', the retarded time ($t' = t - Zc^{-1}$, where c is the velocity of light), r_0, the radial dimension of active laser medium, and A_{12}, the transition moment ($\sec^{-1}$) between states 1 and 2.

We are now in a position to compare the theoretical value[6] of $\sigma_{e^-}(v' = 1) = 1.28 \times 10^{-20}$ cm^2 to the experimental value. The experimental value of σ_{e^-} is determined by fitting Eqs. (A14) and (1) to the experimentally measured energies which range from $W_l = 9 \times 10^{10}$ photons/cm^2 down to less than 10^{10} photons/cm^2 in the (1-4) $Q1$ Werner-band line at 296 °K [see Ref. 4 and Table II(C)]. This fitting indicates $\sigma_{e^-} = (4.0 \pm 0.8) \times 10^{-20}$ cm^2; thus the experimental value is approximately three times

TABLE II. Laser energy.

Gas	Temperature 296 °K	Temperature 90 °K	Detector
(A) Lyman and Werner bands (in units of 10^{13} photons/cm^2)			
H_2	39	41	Film, oxygen attenuator
H_2	4	7	Photodiode, No. 2
H_2	2.3	9	Ionization chamber, TEA filled
para H_2	2.1	9	Ionization chamber, TEA filled
para H_2	>0.5	≫0.7	Film
HD	>0.09	>0.33	Film
D_2	>0.26	≫0.4	Film
D_2	0.9	9	Ionization chamber, TEA filled
D_2	0.8	8	Photodiode, No. 2
(B) $\lambda < 1340$ Å, primarily Werner band (in units of 10^{11} photons/cm^2)			
H_2	1.5	14	Ionization chamber, NO filled
H_2	···	~0.7	Photodiode, No. 1
para H_2	1.4	17	Ionization chamber, NO filled
D_2	1.5	33	Ionization chamber, NO filled
D_2	···	~7	Photodiode, No. 1
(C) Werner band (in units of 10^{11} photons/cm^2)			
H_2	0.57, 5.7[a]	7	Film, methane attenuator
para H_2	<0.1	27	Film, methane attenuator
HD	<0.1	~8	Film, methane attenuator
D_2	<0.1	40	Film, methane attenuator

[a] Atypically large value obtained with a 2-in. entrance inner diameter, 20°, conical section to compress the electron beam. For the concepts related to beam compression, see C. L. Olson, Phys. Fluids 16, 529 (1973); 16, 539 (1973).

larger than the theoretical value. To visualize the amount of optical gain note that the maximum gain at 296 °K, $\exp(N_{\max}\sigma l)$, is $10^{5\pm0.8}$ with the experimentally determined value of σ_{e^-}.

Equation (A6) indicates that saturated gain appears when $W > 6.4\times10^{11}$ photons/cm^2, where W is the laser energy as a function of z with $z < l$. Thus the experimentally observed value of $W_l \leq 9\times10^{10}$ photons/cm^2 has approached but not exceeded the density which marks the onset of saturated gain behavior. As a next step, it is interesting to apply the criterion for saturated gain behavior to this same Werner line at 90 °K.

Equation (A6) indicates saturated gain commences at $W = 3.3\times10^{11}$ photons/cm^2 when operating at 90 °K. Line 4 of Table I(A) and line 1 of Table II(C) show that this energy (for the single strongest line) reasonably well approximates the observed $(2-5)\times10^{11}$ photons/cm^2. Furthermore, if saturated gain behavior were not present, then Eq. (1) indicates W_l would have increased by a factor of 1.1×10^4 due to the exponential dependence on $\sigma(\Delta\lambda)$. The conclusion is that the onset of saturated gain satisfactorily explains why cooling the laser increases the Werner-band output one, but only one order of magnitude. Weaker lines are not limited by saturated gain behavior; hence on this simple basis one anticipates that they increase proportionately more in energy.

The energy emitted in the strong H_2 Lyman-band lines is only moderately increased by cooling to 90 °K, see Table II(A). This is attributed to the laser operating in the saturated gain region with respect to the stronger Lyman lines and the dependence of W_l on σ is very slow for saturated gain:

$$W_l(1+g_2/g_1) \lesssim \tfrac{1}{2}\sigma^{-1} + (l - z_0)N \,. \qquad (2)$$

The above expression is derived as Eq. (A9) in the Appendix where g_2/g_1 is a degeneracy factor. The right-hand terms have the following meanings: $1/2\sigma$ is the total photon density due to unsaturated gain in the region $z < z_0$ and $(l - z_0)N$ is the saturated (photon) gain for $z_0 < z < l$. The transition from unsaturated to saturated gain, at $z = z_0$, is given by Eq. (A6):

$$W\sigma = \tfrac{1}{2}(1+g_2/g_1)(N\sigma z_0)^{1/2} \,. \qquad (3)$$

Take the (5-12) $P3$ Lyman line (at 1613 Å) as an example; saturated gain occurs for $W > 3.8\times10^{11}$ photons/cm^2, two orders of magnitude less than the experimentally measured energy. The experimentally measured $W_l = 4\times10^{13\pm0.5}$ photons/cm^2 is then substituted into Eqs. (2) and (3) in order to find N, which is translated into an excitation cross section $\sigma'_{e^-} = 5\times10^{-20\pm0.4}$ cm^2 by Eq. (A14), and simultaneously, Eq. (3) indicates $z_0 = 90$ cm. The prime on σ'_{e^-} is used to differentiate the present Lyman-band excitation (into the $v' = 5$ state) from the previous Werner-band excitation cross section σ_{e^-}.

Proceeding to the question of the increase in W_l with 90 °K operation, one notes that Eqs. (1) and (3) combine to predict that z_0 decreases to ~45 cm (using the value of $\sigma'_{e^-} = 5\times10^{-20}$ cm^2). In which case, Eq. (2) shows W_l increases only by the ratio ~185 cm/140 cm = 1.32, i.e., 32%. Such an increase is in general agreement with the increases reflected in Table II(A) for 90 °K temperatures.

The experimental value of $\sigma'_{e^-} = 5\times10^{-20\pm0.4}$ cm^2 can now be compared to the theoretical value. Reference 26 shows that theoretically, $\sigma'_{e^-} = 0.5\sigma_{e^-} = 0.64\times10^{-20}$ cm^2. Thus we again observe that the experimental value is several times larger than the theoretical value; to be specific the ratio is $7.8\times10^{\pm0.4}$.

One of the previous approximations appears to contribute about half of the discrepancy. The deduced, in Ref. 6, 3.9% relative cross sections for excitation to ionization holds only for incident (including cascade) electrons of greater than 100-eV energy.[27,28] For electrons of ~20-eV energy, the relative cross-section ratio is several times larger than anticipated from the Born approximation; see Fig. 8, where the shaded region shows the area neglected in the present calculation of σ_{e^-} and σ'_{e^-}. Consequently, the calculation underestimates the number of excitations produced by cascade electrons with near-threshold energies.

Three features indicate that $\sigma(\Delta\lambda)$ is indeed due to Doppler broadening. First, in evaluating the unsaturated gain in the (1-4) $Q1$ Werner line, one is basically checking on the product $\sigma(\Delta\lambda)N(\sigma_{e^-})$ in the exponential term, and $N\sigma$ has been noted to be

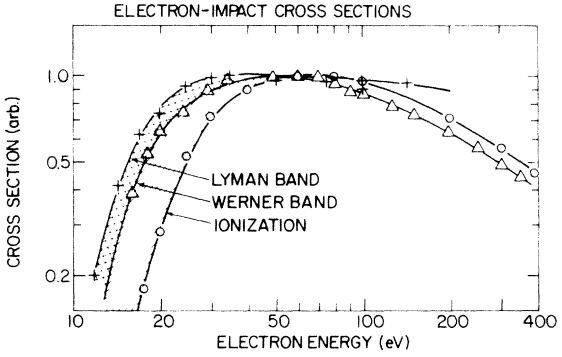

FIG. 8. Relative cross sections for an electron of various energies to produce the designated excitation or ionization. The ionization cross section is from Ref. 30. The excitation cross sections are from Ref. 29.

greater than the theoretical product. Thus any increase in $\Delta\lambda$ to values larger than the Doppler-broadened values would decrease σ and increase the disparity in σ_{e^-} values. The second feature which supports Doppler broadening is the fact that cooling the laser produces the predicted increase in W_l and evidently a decrease in $\Delta\lambda$. The temperature dependence is in the correct direction; however, the onset of saturated gain behavior inhibits establishing the temperature dependence of σ as precisely $T^{-1/2}$. At 90°K, the increased energy available from D_2 as compared to H_2 is the third fact which supports a Doppler-broadening model. The heavier mass of D_2 decreases $\Delta\lambda$ from Eq. (A11), and hence increases σ in Eq. (A10).

In conclusion, and despite the exploratory nature of the present work, a number of fundamental facts about this vuv laser are well established. Among these facts are that the excitation involves primary, secondary, and cascade electrons (with comparable importance); the linewidth is due to Doppler broadening and a simple model only moderately underestimates the inversion density. Using these facts, it has been possible to demonstrate lasing at shorter wavelengths than the previous work,[5] and to increase the Werner-band laser energy over an order of magnitude. Also in demonstrating lasing in HD, D_2, and para H_2, many of the B- and C-state energies have been observed experimentally.

ACKNOWLEDGMENTS

The technical help of R. Linn is gratefully acknowledged. S. Wallace assisted with the power measurements and J. Armstrong contributed many helpful discussions. The reading of numerous spectroscopic plates was facilitated by the computerized densitometer of H. Herd, J. Davies, and R. Buckingham. J. Gerardo, A. Wayne Johnson, and others at Sandia Laboratories contributed to our understanding of electron-beam propagation. G. Herzberg, E. F. Stone, and J. A. R. Samson provided helpful commentary.

APPENDIX

The analysis of amplified spontaneous emission has been previously published,[29] however, the results are expressed below in a form particularly suited to the present pulse excitation. Also, to better visualize the amplification process, explicit assumptions simplify the present equations to analytical expressions.

Because both the electron pulse and fluorescence decay time[30] of H_2 are of the order of 1 to 2 nsec, whereas the time required for light to travel the length of the tube is greater than 6 nsec, propagation effects are important, and it is useful to introduce a retarded time,

$$t' = t - z/c\,. \tag{A1}$$

The electron velocity is ~0.85c and hence, the electron pulse and uv photons remain in near coincidence as they travel down the tube, since the latter is about 2 m long.

The papers cited in Ref. 29 provide much of the theory necessary to describe laser action consisting of short pulses of ASE. The differential equations describing the buildup of the laser photon-flux p are, in general, dependent on the region of the tube one is describing. However, one equation gives the laser power due to both regions I and II. The unit of power is photons/cm^2 sec and the unit of laser energy is photons/cm^2. The differential power gain combines the spontaneous-emission power a with the linear-gain coefficient $\alpha = \sigma N$,

$$dp = N a\,dz + p\alpha\,dz\,, \tag{A2}$$

where N is the net inversion density,

$$N = N_2 - N_1(g_2/g_1)\,. \tag{A3}$$

N_2 and N_1 are the populations of the upper and lower energy levels, respectively. The relationship for $a\,dz$,

$$a\,dz = \pi r_0^2\,dz\;\delta A_{12}/4\pi l^2 = r_0^2 A_{12}\delta\,dz/4l^2\,, \tag{A4}$$

combines the following factors: $\pi r_0^2\,dz$ is the active volume, $(4\pi l^2)^{-1}$ converts the emitted power into a power/cm^2 at a distance l, A_{12} is the spontaneous-emission coefficient (sec^{-1}), and δ is the fraction of (spontaneously emitted) photons with wavelength near line center so that they undergo significant amplification. Reference 29 shows δ equals $(N\sigma z)^{-1/2}$; in the present case $0.2 < \delta < 1$. As justified in Sec. 4c of Ref. 31, the slight dependence of the flux/cm^2 on z is dropped in (A4).

Integration of (A2) plus the appropriate constant of integration yields

$$p(z,t') = \frac{r_0^2 A_{12}\delta\,(e^{N(t')\sigma z} - 1)}{4\sigma l^2}\,,$$

$$= \frac{r_0^2 A_{12}(e^{N\sigma z} - 1)}{4\sigma^{3/2} l^2 N^{1/2} z^{1/2}}\,. \tag{A5}$$

The transition from (the above) unsaturated gain to *saturated gain*, region III of Fig. 2, occurs when W is so great that one-half of the net inversion density is swept out by the passage of the light pulse. This occurs when

$$-\tfrac{1}{2}N = \Delta N = \Delta N_2(1 + g_2/g_1)\,.$$

Also note

$$\Delta N_2 = \int dN_2 = -\int N\sigma p\, dt \approx -N_{\max}\sigma W ,$$

where for purposes of saturated-gain calculations, N is taken equal to its maximum value $N_{\max}$. Combining the above relationships,

$$W\sigma = \tfrac{1}{2}\delta(1 + g_2/g_2)^{-1}$$
$$= [2(1 + g_2/g_1)(N\sigma z_0)^{1/2}]^{-1} . \quad \text{(A6)}$$

The $\delta[= (N\sigma z_0)^{-1/2}]$ factor arises from the fact that only the fraction of N_2 near line center is being depleted by the photon pulse. That is, saturated gain results in "hole burning" in an inhomogeneously broadened transition, cf. Sec's. 15.1, 16.4, and 16.5 of Ref. 32. The half-width at half-maximum (HWHM) width of the present hole is $\delta\Delta\lambda$.

For z beyond the point (defined as z_0) where saturated gain commences, the energy is calculated from $\Delta W = -dz\,\Delta N_2$ and $\Delta N = -N$:

$$dW \approx \frac{N dz}{1 + (g_2/g_1)} (N\sigma z_0)^{1/2} < \frac{N dz}{1 + g_2/g_1} . \quad \text{(A7)}$$

This gain is less than the unsaturated gain, Eq. (A2). In addition, since (A7) does not describe an exponential dependence of W or p on z, the photon flux increases only very slowly with increasing z.

Integration of (A7), from $z = z_0$ to $z = l$ gives

$$(1 + g_2/g_1)W_l \sim \tfrac{1}{2}(N\sigma^3 z_0)^{-1/2} + (l - z_0)(N/\sigma z_0)^{1/2} . \quad \text{(A8)}$$

An upper limit on W_l is obtained from the case of homogeneous broadening, i.e., no hole burning. Actually, a modified form of (A8),

$$(1 + g_2/g_1)W_l < \tfrac{1}{2}\sigma^{-1} + (1 - z_0)N \quad \text{(A9)}$$

gives the best estimate for W_l once the photon pulse has progressed significantly past z_0, because the linewidth will increase rapidly from $\delta\Delta\lambda = \Delta\lambda/(N\sigma z_0)^{1/2}$ to $\sim\Delta\lambda$ (see Fig. 2). The reason is that the unsaturated gain away from line center is greater than the (saturated) gain at line center; consequently the linewidth will increase back to $\sim\Delta\lambda$ in a few e-folding distances, i.e., hole burning disappears.[29]

The above equations provide values of $W_l(N, \sigma)$. The next step is to calculate N and σ as functions of the electron-beam current and electron-excitation cross sections.

The value of σ (on line center) is determined from Eq. (3.2) of Ref. 31:

$$\sigma = \alpha/N = (\pi/\ln 2)^{-1/2} A_{12}\lambda^4/8\pi c\Delta\lambda, \quad \text{(A10)}$$

where λ is the wavelength and the line shape is Gaussian. The linewidth (half-width at half-maximum) $\Delta\lambda$ is determined by Doppler broadening[31]:

$$\Delta\lambda/\lambda = (Mc^2/kT \cdot \ln 2)^{-1/2} = 3.6\times 10^{-7}(T/M)^{1/2}, \quad \text{(A11)}$$

where M is the molecular weight (in amu) and T is the absolute temperature. At 296°K, the Doppler width is 0.005 Å or 0.38 cm^{-1} for $\lambda = 1161$ Å. This width is beyond our spectrographic resolution, so that tests of linewidth must be based upon Eq. (1) via the σ terms. The value of σ(1161 Å) is 1.07×10^{-13} cm^2 and σ(1613 Å) is 1.97×10^{-13} cm^2.

The time dependence of N_2 is expressed by

$$\left.\frac{dN_2}{dt}\right|_z = \frac{jG\sigma_{e^-}}{e} - \frac{N_2}{\tau} - p\sigma N , \quad \text{(A12)}$$

where j is the e-beam current density, G is the gas density, and e is the electron's charge. The quantity $\sigma_{e^-}(v')$ is the *effective cross section* for a 400-keV primary electron to excite a gas molecule into the v' vibrational state, and has been estimated[6] to be 1.28×10^{-20} cm^2 for the upper state of the 1161-Å transition. The fraction N_2/τ gives the loss of N_2 due to spontaneous emission, and $p\sigma N$ is the loss of N_2 due to stimulated emission. The $jG\sigma_{e^-}/e$ term contains one of the most important assumptions, and that is the excitation involves primary electrons in single collisions. This contrasts with other possible models which involve excitations due to collective excitation such as (magnetically) induced currents or instabilities.

The time-dependent beam current density is

$$j(t') = 1.85\times 10^4 \left(\frac{t'}{\tau}\right)^2 e^{-t'/\tau} (\text{in } A/cm^2), \quad \text{(A13)}$$

with $\tau = 0.6$ nsec. This $j(t')$ is equivalent to a total e-beam flux of 1.39×10^{14} electrons/cm^2 and a maximum current density, $j_{\max}$, of 10^4 A/cm^2. Note that there is no j dependence on z; the e beam is considered to propagate without attenuation.

Taking $g_2/g_1 = 1$ (for the $Q1$ branch of the Werner band) and neglecting $p\sigma N$ in region II, allows Eq. (A12) to be written as

$$N = \int_0^{t'} \frac{dN_2}{dt} dt - \int_0^{t'} \frac{dN_1}{dt} dt$$
$$= \int_0^{t'} \left(\frac{jG\sigma_{e^-}}{e} - \frac{1}{\tau}(1 + B)N_2\right) dt .$$

Thus

$$N = 3.7 \frac{j_{\max}}{e}\tau\sigma_{e^-}G\left\{e^{-t'/\tau}\left[\frac{(1+B)}{6}\left(\frac{t'}{\tau}\right)^3 + \frac{B}{2}\left(\frac{t'}{\tau}\right)^2 + B\left(\frac{t'}{\tau}\right) + B\right] - B\right\} . \quad \text{(A14)}$$

The factor B is a sum over Franck-Condon factors and rotational moments which relate the rate of spontaneous emission from state 2 to the rate of filling of state 1, and ranges from ~1 down to ~0.1 for cases of present interest. Taking $B=1$, one calculates that $N_{max} = 0.398 G\sigma_e \tau j_{max}/e$ and occurs at $t/\tau \approx 2$. Without spontaneous emission increasing N_1 at the expense of N_2, then N_{max} is nearly ten times larger, $3.7 G\sigma_e \tau j_{max}/e$, and this shows the detrimental effect of spontaneous emission in region II.

At this point, the goal of increasing the laser power can be formulated in terms of the above analytical expressions. Conceptually, laser power can be increased by increasing z ($\leq l$), N or σ in the exponential term of Eq. (A5). To a major degree, N is determined by the products $\sigma_e j G$. The first factor is essentially constant for a particular electron energy and j is limited by the e-beam generator. The magnitude of G is difficult to increase because the e-beam ceases to propagate for large G, see Sec. II A. The effective value of l is limited to ~2 m because otherwise the electron pulse and light pulse may not remain in synchronism. The reason is that in ~2 m the ($0.85c$) electron pulse will lag the light pulse by ~1 nsec.[33]

The other means of increasing p is to increase σ, the stimulated-emission cross section. While A_{12} and λ are constants for a given transition, Eq. (A10) and (A11) show how σ can be increased by decreasing $\Delta\lambda$, this Doppler-determined linewidth is proportional to $(T/M)^{1/2}$. T is obviously decreased by cooling the laser gas; the equipment for doing this is described in Sec. II B. Also, M can be increased (while still working with the same spectroscopic system) by going from hydrogen to deuterium.

---

†Work supported in part by the U. S. Army Research Office-Durham.

[1]M. Clerc and M. Schmidt, C. R. Acad. Sc. B 272, 668 (1971).

[2]R. W. Dreyfus and R. T. Hodgson, Appl. Phys. Lett. 20, 195 (1972).

[3]E. L. Patterson, J. B. Gerardo, and A. Wayne Johnson, Appl. Phys. Lett. 21, 293 (1972).

[4]R. T. Hodgson and R. W. Dreyfus, Phys. Lett. A 38, 213 (1972).

[5]R. T. Hodgson and R. W. Dreyfus, Phys. Rev. Lett. 28, 536 (1972).

[6]R. W. Dreyfus and R. T. Hodgson, J. Vac. Sci. Technol. 10, 1033 (1973).

[7]A cascade process is defined as the sequence in which a 400-keV primary electron generates intermediate energy (30 eV to 200 keV) secondary electrons which in turn cause multiple excitations and ionizations.

[8]A photograph of the present laser has been reproduced in Industrial Research 14, 27 (1972).

[9]H. A. Koehler, L. J. Ferderber, D. L. Redhead, and P. J. Ebert, Appl. Phys. Lett. 21, 198 (1972); and J. B. Gerardo and A. Wayne Johnson, J. Appl. Phys. 44, 4120 (1973).

[10]The electron-beam generator consists of a Marx high-voltage circuit followed by a Blumlein-circuit voltage doubler and pulse sharpener which delivers a ~600-kV-peak pulse with 30-Ω internal impedance. The pulse is applied to a 30-Ω field-emission diode. A 25-μ Ti anode transmits the ~500-keV electrons into the laser tube with ~10% loss in energy. The peak electron-current density is $\sim 10^4$ A/cm^2.

[11]P. A. Miller, J. B. Gerardo, and P. W. Poukey, J. Appl. Phys. 43, 3001 (1972); and P. A. Miller, J. B. Gerardo, *ibid.* 43, 3008 (1972).

[12]Adsorption coefficients for the simple gases are given by R. D. Hudson, Rev. of Geophys. and Space Phys. 9, 305 (1971), and for TEA by E. Tannenbaum, E. M. Coffin, and A. J. Harrison, J. Chem. Phys. 21, 311 (1953).

[13]Eastman Kodak Company, Rochester, N.Y.

[14]M. J. B. Fairhead and D. W. O. Heddle, J. Phys. E 4, 89 (1971).

[15]W. M. Burton, A. T. Hatter and A. Ridgeley, Amer. Astronaut. Soc. Photo-Bull. 1, 27 (1971) and Appl. Opt. 12, 1851 (1973).

[16]J. A. R. Samson, *Techniques of Vacuum Ultraviolet Spectroscopy* (Wiley, New York, 1967).

[17]D. F. Heath and P. A. Sacker, Appl. Opt. 5, 937 (1966).

[18]No. 4711754, ITT Industrial Laboratories, Fort Wayne, Ind.

[19]S. A. Yakovlev, Instrum. Exp. Tech. 2, 396 (1962); A. H. Laufer, J. A. Pirog, and J. R. McNesby, J. Opt. Soc. Am. 55, 64 (1965).

[20]K. Watanabe, F. M. Matsunaga, and H. Sakai, Appl. Opt. 6, 391 (1967).

[21]K. Watanabe and J. R. Mottl, J. Chem. Phys. 26, 1773 (1957).

[22]W. Kolos and L. Wolniewicz, J. Chem. Phys. 49, 404 (1968).

[23]W. Kolos and L. Wolniewicz, Tables of vibrational and rotational energies for the $B\,^1\Sigma_u^+$, $C\,^1\Pi_u$, and the $^3\Sigma_g^+$ states of the hydrogen molecule (unpublished results).

[24]R. J. Spindler, Jr., J. Quant. Spectrosc. Radiat. Transfer 9, 627 (1969).

[25]The active area is obtained from the densitometer traces *along* the spectral lines.

[26]J. Geiger, Z. Phys. 181, 413 (1964).

[27]E. F. Stone and E. C. Zipf, J. Chem. Phys. 56, 4646 (1972).

[28]B. L. Schram, F. J. DeHeer, M. J. Van der Wiel, and J. Kistemaker, Physica 31, 94 (1965).

[29]A. Yariv and R. C. C. Leite, J. Appl. Phys. 34, 3410 (1963); E. I. Gordon, Bell Syst. Tech. J. 43, 507 (1964), see Eq. (56); and L. Allen and G. I. Peters, J. Phys. A 5, 695 (1972).

[30]J. E. Hesser and K. Dressler, J. Chem. Phys. 45, 3149 (1966) and J. E. Hesser, *ibid.* 48, 2518 (1968).
[31]P. P. Sorokin and W. V. Smith, *The Laser* (McGraw-Hill, New York, 1966).
[32]A. Yariv, *Quantum Electronics* (Wiley, New York, 1968).
[33]Actually the light pulse may propagate at less than c on high-gain transitions, cf. L. Casperson and A. Yariv, Phys. Rev. Lett. 26, 293 (1971). This possibility has been neglected in the present analysis since the propagation velocity would be a function of t' and above the level of the present model.

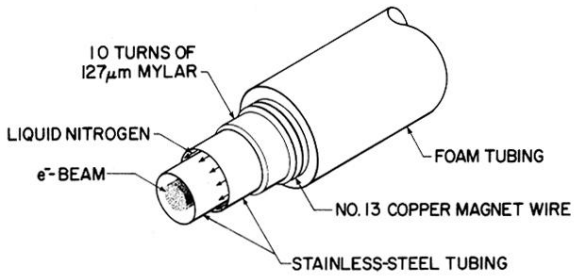

FIG. 4. Cross-sectional view of the laser tube; note the annular space through which liquid nitrogen flows. The diameters of the tube are inner stainless-steel tube, 0.384-in. inner diameter, 0.500-in. outer diameter; outer stainless-steel tube 0.634-in. inner diameter, 0.750-in. outer diameter; and Armoflex (Ref. TM) foam tubing, 0.875-in. inner diameter and 1.875-in. outer diameter. The thermal jacketing is sufficient for liquid nitrogen to flow the 2.3-m length with a consumption of only ~3 liter/h.